

Article

Composition Distribution and Electrochemical Behavior of an Ni₂Al₃ Coating on Q235 Steel

Ningning Li, Minzhi Wang, Gong Zheng, Yongsheng Li and Guang Chen *

Engineering Research Center of Materials Behavior and Design, Ministry of Education, Nanjing University of Science and Technology, Nanjing 210094, China; lnn198898@aliyun.com (N.L.); 15298395693@163.com (M.W.); zhenggong0215@126.com (G.Z.); ysli@njust.edu.cn (Y.L.)

* Correspondence: gchen@njust.edu.cn; Tel./Fax: +86-25-8431-5159

Academic Editor: Hugo F. Lopez

Received: 13 November 2015; Accepted: 8 March 2016; Published: 11 March 2016

Abstract: An Ni₂Al₃ coating was prepared via the electrodeposition of nickel followed by pack aluminization. Polarization curve and electrochemical impedance spectroscopy were performed to study the room temperature corrosion behavior of the coating in a 3.5 wt. % NaCl solution. The long-term impedance of the coating was also investigated after immersion for 30 days. Results show that the Ni₂Al₃ coating possessed lower corrosion current density (I_{corr}) and higher polarization resistance (R_p) than the substrate in the solution. The Bode plots of the coating showed two time constants after the long-term immersion. Pitting corrosion was found on the coating surface.

Keywords: Ni₂Al₃ coating; polarization curve; electrochemical impedance spectroscopy; pitting corrosion

1. Introduction

Nickel-aluminide type coatings, such as Ni₂Al₃, NiAl, and Ni₃Al, are widely used for protecting the nickel-base superalloy against high-temperature oxidation [1–3] or carburization [4]. Further, the nickel-aluminide coatings can also protect other metal substrates with different preparation methods. For example, the SHS (self-propagating high-temperature synthesis) casting route can prepare a Ni₃Al coating to protect carbon steel [5], a plasma-sprayed Ni₃Al coating can protect boiler tube steels [6,7], a mechanical alloying to format nanostructure NiAl can defend carbon steel [8], and a two-step process to make nickel aluminide/nickel hybrid coatings can shield alloy steel [9] or TiAl alloy [10]. Compared to the other methods mentioned above, the two-step process can aluminize at low temperature by pack aluminization of preliminarily nickel-coated samples [9]. Due to the simple composition and single structure of the nickel layer, the Ni/Al diffusion coefficient is higher than that of a superalloy [11].

The Ni₂Al₃ coating has been previously prepared by the two-step method mentioned above [9,12]. The main concern, therefore, is with high temperature oxidation property rather than the room corrosion [9]. Studying the corrosion behavior of the coating in Cl⁻ solution can explore its potential application in the seawater. Compared with the results of ocean exposure experiment, the NaCl (3.5 wt. %) solution is widely used to simulate the ocean environment [13–16]. An electrochemical technique is commonly adopted to characterize the corrosion behavior of material [13,17–23].

The aim of the present work is to investigate the room temperature corrosion behavior of the Ni₂Al₃ coating in a Cl⁻ solution (3.5 wt. % NaCl). Polarization curve and electrochemical impedance spectroscopy (EIS) were used to clarify the electrochemical behavior of the Ni₂Al₃ coating.

2. Experimental Section

2.1. Sample Preparation

The Q235 steel serving as the substrate was cut to a size of 10 mm × 10 mm × 2 mm ($L \times W \times H$). All of the specimens were ground with emery paper from 120 to 800 grits, then polished with alumina suspension, cleaned with acetone and distilled water, and finally immediately dried. The substrate was first plated with nickel using direct current electrodeposition in a Watts bath. After plating, the specimens were aluminized using pack cementation at 650 °C for 20 h. The pack powder mixture was composed of Al, AlCl₃ (anhydrous), and Al₂O₃ powder.

2.2. Electrochemical Tests

The electrochemical tests were conducted with the electrochemical working station (CHI604D, Chenhua, Shanghai, China). All measurements were tested in a Cl[−] solution, namely, a 3.5 wt. % NaCl solution at room temperature. A platinum electrode and a saturated calomel electrode (SCE) were used as the counter and the reference electrode, respectively. The specimens were embedded in epoxy resin with an exposed working area of 1 cm² ($L \times W$) as the working electrodes. Before electrochemical tests, the coated samples were soaked for 30 min in the electrolyte solution. A polarization curve measurement was performed at potentials from −500 to +500 mV *versus* open circuit potential. In order to study the coating failure mechanism, it was immersed for 30 days to test the impedance spectrum.

3. Results and Discussion

3.1. Coating Characterization

Figure 1 shows the XRD pattern of the surface coating on the substrate. It indicates that the surface coating mainly consisted of the Ni₂Al₃ phase. Figure 2 presents the morphology and composition of the Ni₂Al₃ coating surface. As shown in Figure 2a, the coating surface is smooth. The atomic percentage of Ni is 41.17 at. %, while the content of Al is 58.83 at. % (Figure 2b). The atomic ratio of Ni to Al is close to 2/3, which is consistent with the result of XRD.

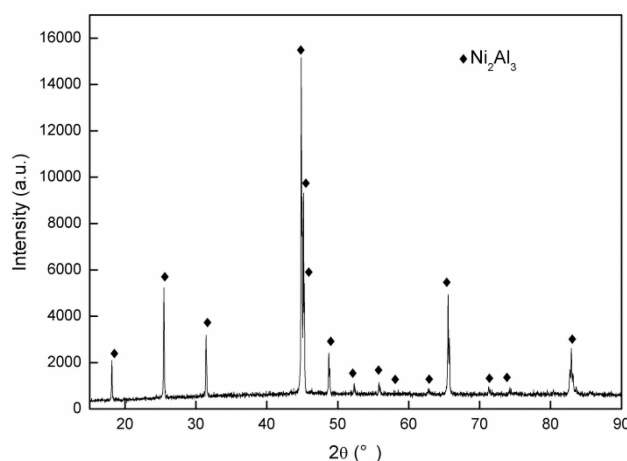


Figure 1. The XRD pattern of the Ni₂Al₃ coating.

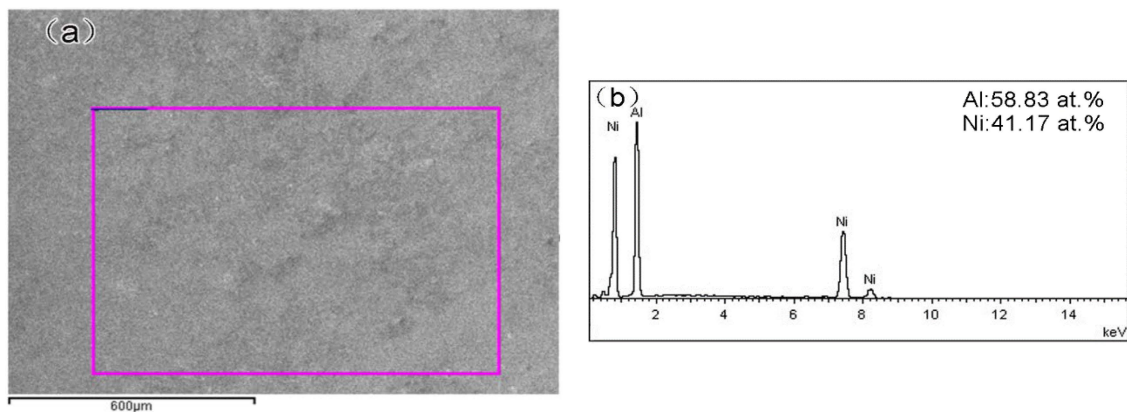


Figure 2. The morphology (a) and composition (b) of the Ni_2Al_3 coating surface.

The coating cross-section morphology is smooth with no apparent pore defects, as can be seen in Figure 3a. The composition of Ni and Al are stable from the surface to about $30\ \mu\text{m}$ into the internal, then the Ni decreases and the Al increases in the diffusion zones, where Fe is present, as shown in Figure 3b. The content of Ni and Al are gradually reduced to zero deep into the substrate (about $55\ \mu\text{m}$). The rest is Fe. The results show that the Ni_2Al_3 coating was successfully prepared by using the two-step process; the thickness of the coating is about $30\ \mu\text{m}$, while the diffusion zone is $20\ \mu\text{m}$ thick.

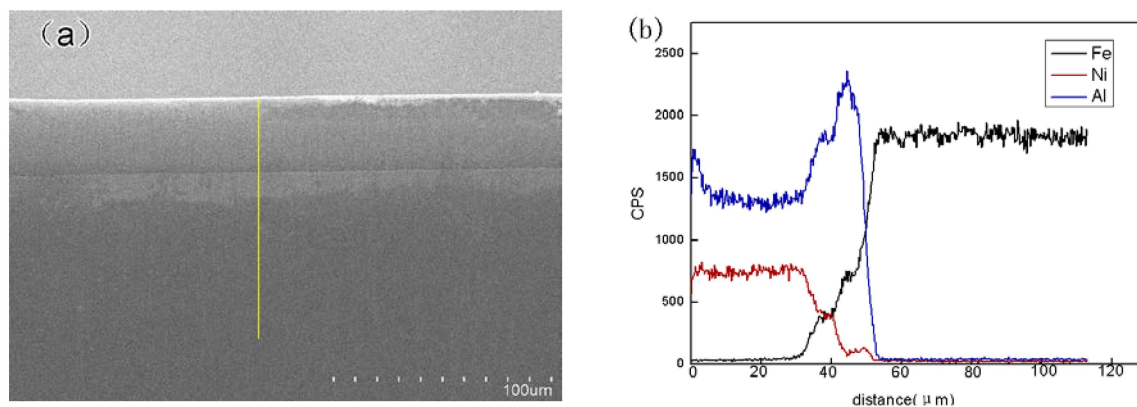


Figure 3. Cross section (a) and composition (b) of a line scan of the Ni_2Al_3 coating.

3.2. Electrochemical Behavior

The polarization curves of different material in the 3.5 wt. % NaCl solution are shown in Figure 4. The anodic slope β_a and cathodic slope β_c can be obtained from the Tafel region of the polarization curves. The corrosion current density I_{corr} and polarization resistance R_p can also be directly obtained (Table 1). The Stern-Geary constant B [24] is calculated by the equation:

$$B = \beta_a \times \beta_c [2.3(\beta_a + \beta_c)]^{-1} \quad (1)$$

The relation between I_{corr} and R_p is given [24]:

$$I_{\text{corr}} = B/R_p \quad (2)$$

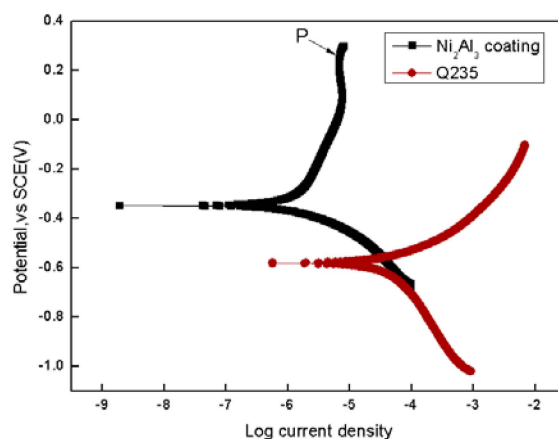


Figure 4. The polarization curves of the Ni_2Al_3 coating and Q235 steel in the 3.5 wt. % NaCl solution.

Table 1. Electrochemical corrosion parameter values for the Ni_2Al_3 coating and Q235 steel in the 3.5 wt. % NaCl solution by polarization curve.

Materials	β_a (V)	β_c (V)	R_p ($\text{ohm} \times \text{cm}^{-2}$)	I_{corr} ($\mu\text{A} \times \text{cm}^{-2}$)
Q235	0.822	0.121	1083	42.27
Ni_2Al_3 coating	0.116	0.213	9626	3.401

The B values can be calculated by Equation (1). From the calculated data, it can be seen that the relationship between I_{corr} , R_p and B is roughly in accordance with Equation (2). The coating corrosion current density (I_{corr}) is about 1/28 of that of the substrate (see Table 1). At the same potential, the I_{corr} of the coating is much lower than that of the substrate. Meanwhile, the inflection point (point P) of the polarization curves in Figure 4 should be noticed, since the current density suddenly increases after the point P. In other words, the passive state (before point P) is converted into the active state (after point P) according to the change of the current density.

The corrosion resistance can also be evaluated by means of the electrochemical impedance spectroscopy (EIS) measurement. Figure 5 shows the equivalent circuit models in order to analyze the EIS results. Each parameter of the models is represented as following: R_s is the solution resistance, C_{dl} is the double layer capacitance, R_{ct} is the charge transfer resistance at the surface/electrolyte interface, C_c is the coating capacity, and R_c is the coating resistance. Y_0 ($\text{ohm} \cdot \text{cm}^{-2} \cdot \text{s}^n$) and n ($0 \leq n \leq 1$) are the two parameters that characterize both C_{dl} and C_c . Y_0 represents the base admittance of the constant phase element (CPE), where n is the exponent, which can be used as a gauge of surface heterogeneity [25]. Figures 6 and 7 show the Nyquist and Bode plots of the experimental and fitted EIS curves of the coating at different times. The extracted impedance parameters analyzed by the EIS analyzer software from the plots are summarized in Table 2.



Figure 5. The equivalent circuits to fit long-term EIS results for: (a) early stage; (b) middle-late stage.

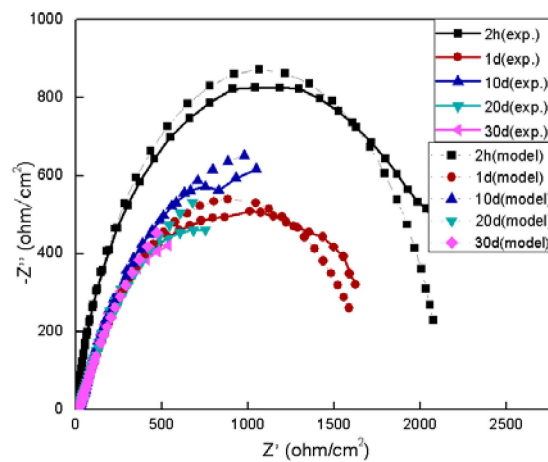


Figure 6. The Nyquist of the Ni₂Al₃ coating in different soaking times. The symbols delegate the experimental results, and the lines delegate the model results.

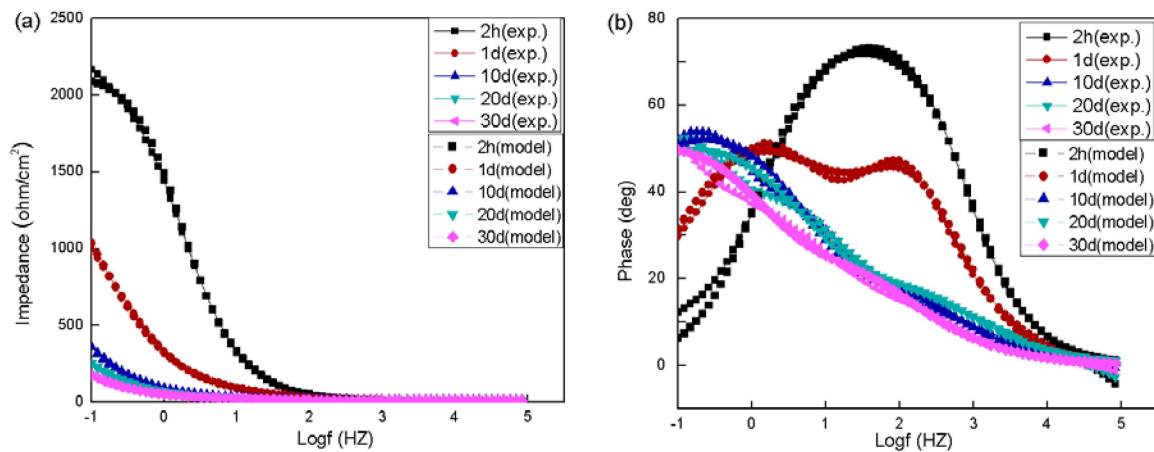


Figure 7. The Bode of the Ni₂Al₃ coating in different soaking times. The symbols delegate the experimental results, and the lines delegate the model results. (a) Impedance diagram; (b) phase diagram.

Table 2. EIS parameters for the Ni₂Al₃ coating at different immersion times.

Time	R_s	C_c		R_c	C_{dl}		R_{ct}
	(ohm·cm ⁻²)	γ_0 (ohm·cm ⁻² ·s ⁿ)	n	(ohm·cm ⁻²)	γ_0 (ohm·cm ⁻² ·s ⁿ)	n	(ohm·cm ⁻²)
2 h	6.765	-	-	-	8.089×10^{-5}	0.8696	2144
1 d	8.331	1.803×10^{-4}	0.8232	78.65	6.963×10^{-4}	0.6837	1691
10 d	11.59	1.177×10^{-3}	0.655	19.32	2.48×10^{-3}	0.6943	2225
20 d	8.072	1.401×10^{-3}	0.6322	14.33	3.727×10^{-3}	0.6395	2238
30 d	9.741	3.491×10^{-3}	0.5997	32.8	4.327×10^{-3}	0.6828	2459

According to the EIS results, it can be understood that at the first 2 h of immersion, the Nyquist and Bode plots of the coating show only one time constant that is typically an indication of uniform corrosion occurrence on the coating surface (Figures 6 and 7b). The results indicate that there is only one reaction interface between the coating and solution. As time passes by, there are two time constants emerged in Figure 7b. These two time constants represent two interfaces: one is the oxide film and coating surface, and the other is the oxide film and electrolyte solution. These results are consistent with the above-mentioned equivalent circuit models (Figure 5).

There are two interfaces indicating two interface reactions. One is the formation of oxide film, and the other is the destruction of the oxide film. At the beginning of the corrosion process, the formation of oxide film is faster than that of the destruction. Then, the destruction of oxide film is accelerated due to the constant infiltration of the corrosion solution. At this period, the value of R_{ct} decreases (see Table 2). Finally, the destruction of oxide film is still faster than that of formation. Therefore, the coating corrosion resistance increases, which is caused by the accumulation of the corrosion products; corrosion products inhibit the solution ions (Cl^-), penetrating the coating to corrode the substrate, which leads to an increase in the value of R_{ct} .

The variation tendency of R_{ct} verified our analysis of the coating corrosion process very well (Table 2). The larger the R_{ct} , the better the corrosion resistance.

After 30 d of immersion, the coating surface became gray and dark. The XRD pattern of the corrosion products on the coating surface is shown in Figure 8. The main corrosion products are made up of Ni_2Al_3 , Al_2O_3 , and $AlCl_3O_{12}$. The Al_2O_3 oxide film is formed on the surface in contact with the aqueous solution. The existence of $AlCl_3O_{12}$ shows that the corrosion is mainly caused by the Cl^- ion.

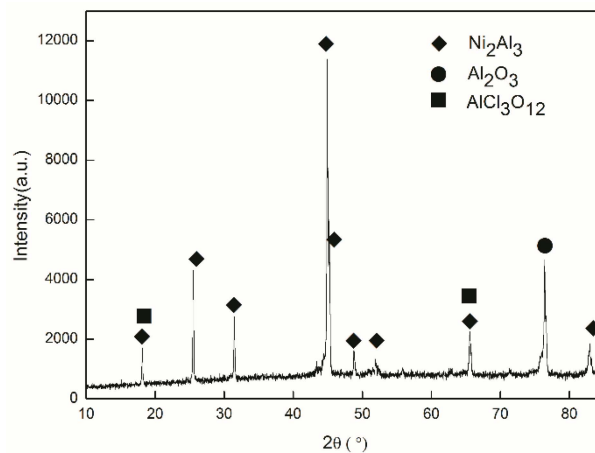


Figure 8. XRD pattern of the corrosion products on the coating surface after 30 d immersion.

The morphology of the corrosion products surface is shown in Figure 9a. They randomly distributed in granular form. When the corrosion products are removed, it is found that pitting occurs (Figure 9b).

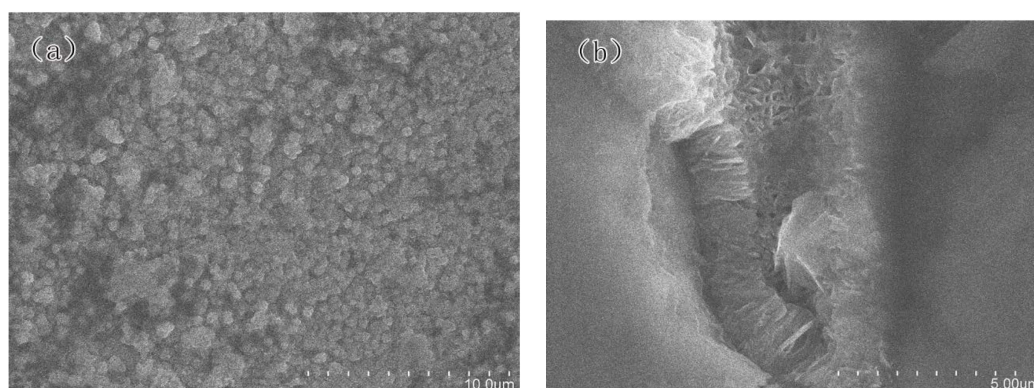


Figure 9. The morphology of corrosion products on the coating surface. (a) Low image; (b) high image.

4. Conclusions

The Ni_2Al_3 coating was successfully prepared on Q235 steel, and its room temperature corrosion behavior in a 3.5 wt. % NaCl solution was studied. Polarization curve and electrochemical impedance

spectroscopy measurements were analyzed. It was shown that the Ni₂Al₃ coating has lower corrosion current density (I_{corr}) and higher polarization resistance (R_p) compared to the substrate steel. Pitting corrosion was found in the coating surface.

Acknowledgments: The authors gratefully acknowledge the financial support of the Jiangsu Province Ordinary University Graduate Student Research Innovation Project of China (CXLX12-0193), the Foundation of Jiangsu Key Laboratory of Advanced Structural Materials and Application Technology (No. ASMA201403), and the Cooperative Innovation Fund of Jiangsu Province (No. BY2014004-09).

Author Contributions: Ningning Li conceived, designed and performed the experiments, analyzed the data and wrote the manuscript. Minzhi Wang and Gong Zheng revised the manuscript. Yongsheng Li helped perform the analysis with constructive discussions. Guang Chen contributed to the conception of the study and approved the final version.

Conflicts of Interest: The authors declare no conflict of interest.

References

- Goward, G.W.; Boone, D.H. Mechanisms of formation of diffusion aluminide coatings on nickel-base superalloys. *Oxid. Met.* **1971**, *3*, 475–495. [[CrossRef](#)]
- Shirvani, K.; Firouzi, S.; Rashidghamat, A. Microstructures and cyclic oxidation behavior of Pt-free and low-Pt NiAl coatings on the Ni-base superalloy Rene-80. *Corros. Sci.* **2012**, *55*, 378–384. [[CrossRef](#)]
- Hou, S.J.; Zhu, S.L.; Zhang, T.; Wang, F.H. A magnetron sputtered microcrystalline β -NiAl coating for SC superalloys. Part I. Characterization and comparison of isothermal oxidation behavior at 1100 °C with a NiCrAlY coating. *Appl. Surf. Sci.* **2015**, *324*, 1–12. [[CrossRef](#)]
- Wang, Y.; Chen, W. Microstructures, properties and high-temperature carburization resistances of HVOF thermal sprayed NiAl intermetallic-based alloy coatings. *Surf. Coat. Technol.* **2004**, *183*, 18–28. [[CrossRef](#)]
- La, P.Q.; Bai, M.W.; Xue, Q.J.; Liu, W.M. A study of Ni₃Al coating on carbon steel surface via the SHS casting route. *Surf. Coat. Technol.* **1999**, *113*, 44–51. [[CrossRef](#)]
- Sidhu, B.S.; Puri, D.; Prakash, S. Characterisations of plasma sprayed and laser remelted NiCrAlY bond coats and Ni₃Al coatings on boiler tube steels. *Mater. Sci. Eng. A* **2004**, *368*, 149–158. [[CrossRef](#)]
- Sidhu, B.S.; Prakash, S. Evaluation of the corrosion behavior of plasma-sprayed Ni₃Al coatings on steel in oxidation and molten salt environments at 900 °C. *Surf. Coat. Technol.* **2003**, *166*, 89–100. [[CrossRef](#)]
- Mohammadnezhad, M.; Shamanian, M.; Enayati, M. Formation of nanostructured NiAl coating on carbon steel by using mechanical alloying. *Appl. Surf. Sci.* **2012**, *263*, 730–736. [[CrossRef](#)]
- Xiang, Z.D.; Rose, S.R.; Datta, P.K. Low-temperature formation and oxidation resistance of nickel aluminide/nickel hybrid coatings on alloy steels. *Scr. Mater.* **2008**, *59*, 99–102. [[CrossRef](#)]
- Katsman, A.; Ginzburg, A.; Werber, T.; Cohen, I.; Levin, L. Nickel-aluminide coating of TiAl by a two-stage process. *Surf. Coat. Technol.* **2000**, *127*, 220–223. [[CrossRef](#)]
- Hickl, A.J.; Heckel, R.W. Kinetics of phase layer growth during aluminide coating of nickel. *Metall. Trans. A* **1975**, *6*, 431–440. [[CrossRef](#)]
- Xiang, Z.D.; Datta, P.K. Formation of nickel aluminide/nickel hybrid coatings on alloy steels by two step process of nickel plating and low temperature pack aluminisation. *Mater. Sci. Technol.* **2009**, *25*, 733–738. [[CrossRef](#)]
- Mohanty, U.S.; Lin, K.L. Electrochemical corrosion study of Sn-X Ag-0.5 Cu alloys in 3.5% NaCl solution. *J. Mater. Res.* **2007**, *22*, 2573–2581. [[CrossRef](#)]
- Kaiser, M.S.; Dutta, S. Corrosion behavior of aluminium engine block in 3.5% NaCl solution. *J. Mater. Sci. Chem. Eng.* **2014**, *2*, 52–58.
- Mohanty, U.S.; Lin, K.L. Electrochemical corrosion behavior of lead-free Sn-8.5 Zn-X Ag-0.1 Al-0.5 Ga solder in 3.5% NaCl solution. *Mater. Sci. Eng. A* **2005**, *406*, 34–42. [[CrossRef](#)]
- Lv, D.M.; Ou, J.F.; Xue, M.H.; Wang, F.J. Stability and corrosion resistance of superhydrophobic surface on oxidized aluminum in NaCl aqueous solution. *Appl. Surf. Sci.* **2015**, *333*, 163–169. [[CrossRef](#)]
- Souza, V.A.D.; Neville, A. Linking electrochemical corrosion behavior and corrosion mechanisms of thermal spray cermet coatings (WC-CrNi and WC/CrC-CoCr). *Mater. Sci. Eng. A* **2003**, *352*, 202–211. [[CrossRef](#)]
- Hsu, R.W.W.; Yang, C.C.; Huang, C.A.; Chen, Y.S. Electrochemical corrosion properties of Ti-6Al-4V implant alloy in the biological environment. *Mater. Sci. Eng. A* **2004**, *380*, 100–109. [[CrossRef](#)]

19. Li, C.; Zheng, Y.F.; Zhao, L.C. Electrochemical corrosion behavior of Ti₄₄Ni₄₇Nb₉ alloy in simulated body fluids. *Mater. Sci. Eng. A* **2006**, *438–440*, 504–508. [[CrossRef](#)]
20. Javadian, S.; Yousefi, A.; Neshati, J. Synergistic effect of mixed cationic and anionic surfactants on the corrosion inhibitor behavior of mild steel in 3.5% NaCl. *Appl. Surf. Sci.* **2013**, *285*, 674–681. [[CrossRef](#)]
21. Wang, J.F.; Li, Y.; Huang, S.; Zhou, X.A. Study of the corrosion behavior and the corrosion films formed on the surfaces of Mg-*x* Sn alloys in 3.5 wt. % NaCl solution. *Appl. Surf. Sci.* **2014**, *317*, 1143–1150. [[CrossRef](#)]
22. Madaoui, N.; Saoula, N.; Zaid, B.; Saidi, D.; Ahmed, A.S. Structural, mechanical and electrochemical comparison of TiN and TiCN coatings on XC48 steel substrates in NaCl 3.5% water solution. *Appl. Surf. Sci.* **2014**, *312*, 134–138. [[CrossRef](#)]
23. Bai, Z.H.; Xia, Y.M.; Qiu, F.; Liu, Y.Y.; Hu, W.; Jiang, Q.C. Effects of RE_{*x*}O_{*y*} addition on corrosion behavior of the Al-Cu alloys in 3.5 wt. % NaCl solution and pH = 4 acid solution. *Appl. Surf. Sci.* **2014**, *307*, 153–157. [[CrossRef](#)]
24. Stern, M.; Geary, A.L. Electrochemical polarization: I. A theoretical analysis of the shape of polarization curves. *J. Electrochem. Soc.* **1957**, *104*, 56–63. [[CrossRef](#)]
25. Yin, Z.F.; Zhao, W.Z.; Lai, W.Y.; Zhao, X.H. Electrochemical behaviour of Ni-base alloys exposed under oil/gas field environments. *Corros Sci.* **2009**, *51*, 1702–1706. [[CrossRef](#)]



© 2016 by the authors; licensee MDPI, Basel, Switzerland. This article is an open access article distributed under the terms and conditions of the Creative Commons by Attribution (CC-BY) license (<http://creativecommons.org/licenses/by/4.0/>).